Subsonic Single-Phase Flow in a Gun Simulator

A. F. Bicen,* L. Khezzar,* and J. H. Whitelaw*
Imperial College of Science and Technology, London, England

Reported here are the time-resolved and ensemble mean and rms fluid velocities obtained by laser Doppler anemometry in a subsonic gun simulator with an inert single-phase flow and a projectile exit velocity of 40 m/s. The results presented also include the time-resolved measurements of the projectile velocity and breech pressure. The results show that, based on measured breech-pressure record, the calculated projectile velocities are almost exactly equal to the measured values and confirm that the friction of the system is negligible. Fluid velocity traces, together with ensemble mean and rms velocity profiles, indicate the presence of a wall boundary layer occupying up to 20% of the tube radius and having a growth rate similar to that of steady turbulent boundary layers. The nature of velocity fluctuations and the shape of velocity profiles inside the boundary layer also suggest that the boundary layers are turbulent in the wake of the projectile.

Nomenclature

A = cross-sectional area of projectile
a = local speed of sound
d = tube diameter
F_r = friction force
g = acceleration of gravity
m = mass of projectile
P_a = atmospheric pressure (back pressure)
P_b = breech pressure
P_0 = absolute initial pressure
R = tube radius
r = distance from cylinder wall
t = time
U = ensemble mean axial velocity
U_c = centerline mean velocity
u' = ensemble rms axial velocity
V_p = projectile velocity
x = Eulerian coordinate measured from breech (fluid)
z = Lagrangian coordinate (projectile)
z_0 = initial chamber length
γ = isentropic coefficient
δ = boundary-layer thickness
ρ_0 = initial fluid density

Introduction

THE flowfield behind the projectile in a real gun is characterized by high velocities of the solid and gas phases and by exothermic reactions, with temperatures[1] up to 3000 K, and unsteady boundary layers at the walls behind the projectile. The short duration of the projectile travel within the barrel adds to the difficulty of accurate measurements of the high-speed transient phenomena. A related program of research has recently been recommended,[2] involving experiments with simulators that permit the generation of well-controlled flows, starting with more simplified single-phase inert flows and advancing progessively toward more complex two-phase reacting flows. A strong interest is also being shown by the computational communities[3,4] that, it is hoped, will provide the means of interpolation and extrapolation of the experimental results. For example, Heiser[4] has obtained encouraging agreement with the experimental results of Ref. 5 by solving the full Navier-Stokes equations for laminar flows.

The work presented here describes inert single-phase measurements of the pressure and projectile and fluid velocities in a subsonic gun simulator. The model gun has a preburned propellant and constant diameter in ballistic phraseology. It constitutes a continuation and improvement of the work reported in Ref. 5. The wall shear layers that existed in the gas expanding behind a projectile of Ref. 5 were found to be less than 1% of the tube diameter; thus, it was difficult to provide detailed results that would clarify the nature of the unsteady boundary layer. In the present study, the length of the travel distance of the projectile has been extended, thus allowing the boundary layers to grow more than in the previous study. Little is known about transient boundary layers.[6,7] Consequently, particular attention is paid to the nature of the ensuing boundary layers, since their behavior accounts for the momentum and heat transfer to the wall of the barrel. In addition, a novel optical technique has been developed and used successfully to obtain the projectile velocity as a function of space and time. This work also represents a stage in a program of research aimed at evaluating measurement techniques in configurations with high-speed, two-phase flow.

Experimental Techniques

Flow Configuration

The flow arrangement shown in Fig. 1 is similar to that in Ref. 5, but it has a projectile travel of $14d$ (as opposed to $4d$) and a lighter projectile that can achieve higher velocities within the range of the initial pressures used in the Ref. 5 test.

The projectile is secured in position inside a tube of 76.5 mm diameter and is pressurized by compressed nitrogen. After the gas becomes quiescent, the projectile is released and travels a distance of about 1 m ($\simeq 13d$) inside the tube (which is machined to high precision). The initial chamber of 306 mm ($4d$) in length is fabricated from plexiglass to provide optical access for the laser Doppler anemometer. The remainder of the barrel is made of mild steel, with four small circular plexiglass windows, as shown in Fig. 1, to allow velocity measurements to be made at axial distances of approximately 7, 10, 13, and $16d$ from the breech. A lock mechanism has been designed to secure the projectile under the pressure load at its starting position and to release it smoothly and spontaneously without causing jitter. The in-

Received Sept. 24. 1986; revision received April 6, 1987.

*Mechanical Engineering Department.

itial sealing of the chamber is achieved by means of an O-ring fitted around the inner surface of the tube, against which the projectile rests at its start position. After the projectile is released and during its travel inside the barrel, two plastic rings fitted on the projectile prevent blowby of the compressed gas. The projectile is 250 mm long and weighs 0.953 kg. The top and bottom parts are made of an aluminium alloy and a central plexiglass section houses a linear graticule for projectile velocity measurements. At the end of its travel, the projectile is decelerated by compression of the air inside the lower part of the barrel. A control valve fitted at the bottom and connected to a compressed air supply is used to return the projectile to its lock-and-start position at the top of the barrel.

Measurement Systems

Emphasis has been placed on the development of an improved method for measuring the projectile velocity. The chosen optical technique makes use of a linear graticule and eliminates the need for the alternative mechanically complex rack-and-gear mechanism of Ref. 5, thus removing the ambiguity in the associated friction force. The graticule inside the projectile consists of 25 lines/in. The measuring systems are shown in Fig. 1.

For the projectile velocity measurements, the instrumentation comprises a 5 mW He-Ne laser, a lens to focus the beam at its waist on the graticule, a pinhole, and another lens to focus the emerging beam onto a photodiode. The lens/pinhole combination reduces the field of view of the diode to a minimum possible for system operation and thereby reduces the sensitivity of the system to unwanted optical noise from reflections and flares. The graticule moves with the projectile and transmits a pulse train whose period coincides with the chopping of the laser beam by the graticule. The output signal of the diode is converted to a square wave by a Schmitt trigger, which is compatible with digital logic. The individual periods are timed by a high-frequency clock and stored in a buffer memory from which the velocity of the projectile can be computed during the part of the cycle corresponding to the transient time of the projectile across the selected window. By repeating the measurements at each of the four windows, a velocity-travel curve for the whole cycle can be assembled.

For measurements of the fluid velocity, a dual-beam laser Doppler anemometer operated in the forward-scatter mode was used. The anemometer consisted of a 32 mW He-Ne laser, focussing lens, rotating diffraction grating, collimating lens, collecting lens, and photomultiplier, as shown in Fig. 1. The principal characteristics of the optical system are given in Table 1. Silicone oil particles were used as scattering particles and were introduced in the initial chamber prior to charging of the volume at the required release pressure. The output of the photomultiplier was bandpass filtered to remove the pedestal and the high-frequency noise and input to a purposely built frequency counter with an 8/16 validation logic and a cycle time of 45 μs. The frequency counter was interfaced to a microcomputer that sampled the digital output of the counter and stored it in memory at a rate of $\simeq 10$ kHz. The time information corresponding to each frequency count was obtained from a programmable timer module, which was activated to time at a rate of 477 kHz after the first 2 mm of the projectile travel. The data were subsequently processed by the microcomputer to determine and display the variation of velocity as a function of time.

The initial pressure used was 8 bars and achieved with low-grade nitrogen taken from a pressurized cylinder. The initial pressure and the breech pressure record during the cycle were measured with a precision of ± 0.002 bars, using a piezoelectric transducer and a charge amplifier whose analog output was digitized and interfaced with the microcomputer.

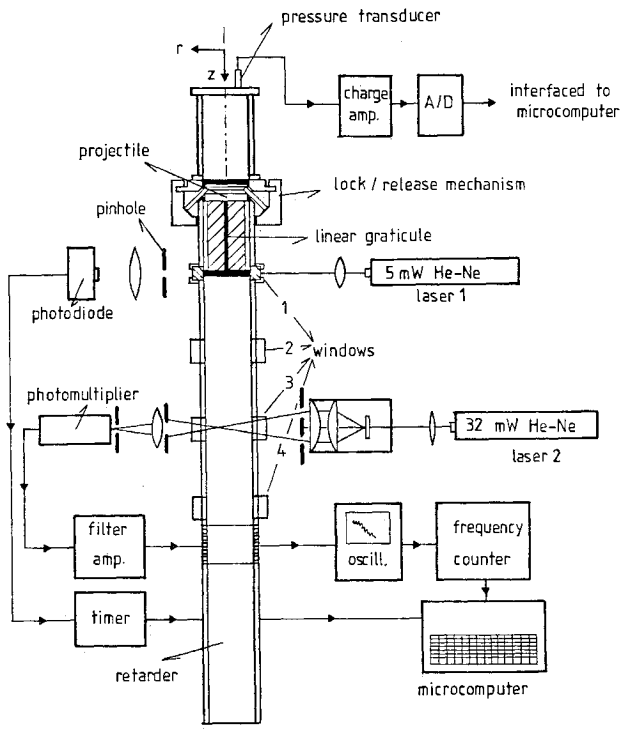

Fig. 1 Schematic diagram of experimental test setup.

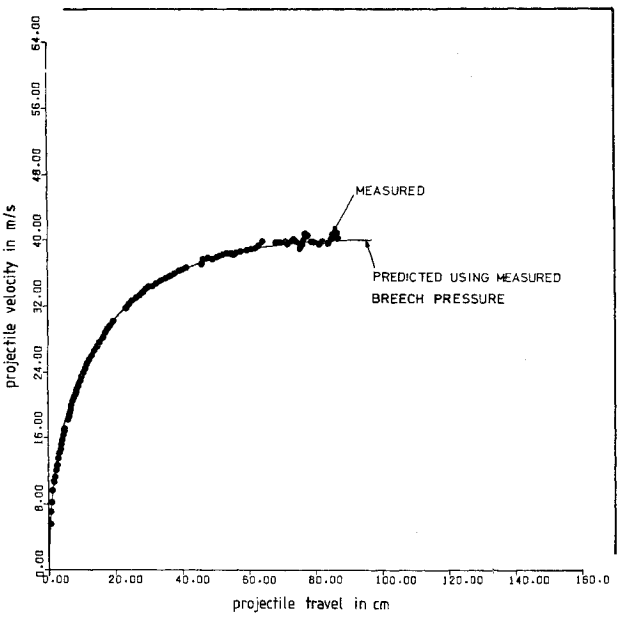

Fig. 2 Measured and predicted projectile velocity-travel curves.

Table 1 Principal characteristics of optical system

Half-angle of intersection of beams	6.10 deg
Fringe spacing	2.99 μm
Length of probe volume at e^{-2} intensity level	0.908 mm
Diameter of probe volume at e^{-2} intensity level	0.097 mm
No. of fringes within e^{-2} intensity level	34

Results and Discussion

Projectile Dynamics

Figure 2 shows the measured velocity-travel curve of the projectile together with the curve calculated from the measured breech pressure-time record. The measured traces were found to be repeatable within 1% from cycle to cycle over a large number of cycles and the problem of varying friction encountered with the previous experimental setup of Ref. 5 has been removed. The projectile accelerates rapidly from rest to reach its exit velocity of about 40 m/s in about 30 ms. The acceleration of the projectile is greatest at the start of the motion and decreases monotonically to reach almost zero at the end of the cycle.

The motion of the projectile can be determined if the pressure acting on its base is known. The relation that gives the base pressure as a function of the breech pressure acting along a characteristic line is[8]

$$P_{\text{base}} = P_{\text{breech}} \cdot \left(1 - \frac{\gamma - 1}{2} \cdot \frac{V_p}{a}\right)^{2\gamma/(\gamma-1)} \tag{1}$$

The projectile motion as a function of the breech pressure is then given by the equations

$$\frac{dV_p}{dt} = A \cdot m^{-1} \cdot P_b \cdot \left[1 - \frac{\gamma - 1}{2} V_p \left(\frac{\gamma}{\rho_0} P_b^{(\gamma-1)/\gamma} \times P_0^{1/\gamma}\right)^{-1/2}\right]^{2\gamma/(\gamma-1)} - P_a \cdot A \cdot m^{-1} + g + F_r \cdot m^{-1} \tag{2}$$

$$V_p = \frac{dz}{dt} \tag{3}$$

In Eq. (2), the compressibility effect on the atmospheric side has been ignored since, under the present conditions, it does not contribute more than 0.5% to the exit projectile velocity (e.g., see Ref. 9). Preliminary pressure measurements obtained near the muzzle verified this assumption.

Equations (2) and (3) constitute a coupled set of simultaneous ordinary differential equations in z and V_p in terms of t and can be solved numerically by a standard fourth-order Runge-Kutta algorithm. The friction force term in Eq. (2) is taken to be equal to zero since no a priori model for it exists. The calculated values for V_p in Fig. 2 indicate a value at the exit position of 40.0 m/s, which is almost exactly equal to the measured value and thus suggests a negligible friction force. This fact assumes particular significance for the numerical predictions, which obviates the need for considerations of the wall friction force.

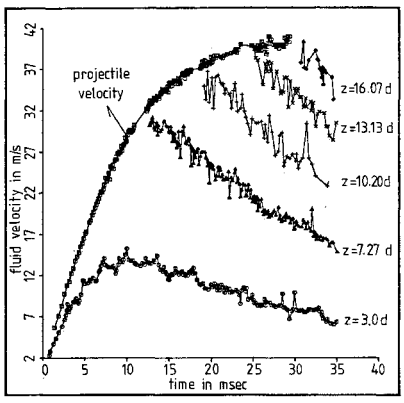

Fig. 3 Centerline velocity traces at different axial stations.

Fluid Velocity Measurements

The centerline velocity traces of the fluid together with the projectile velocity measurements are shown in Fig. 3 for the axial stations of $x=3d$, $7.27d$, $10.20d$, $13.13d$, and $16.07d$. At $x=3d$, which corresponds to the position inside the initial chamber, the fluid velocity increases monotonically with time to reach a maximum of 14 m/s at around 10 ms. No fluctuations are present during the acceleration period. After reaching the maximum, the velocity decreases to 7 m/s on average at about 35 ms and fluctuations, although of low magnitude, start to appear with decreasing acceleration. The fluid velocities immediately behind the projectile have been measured at the subsequent axial stations and increase in accordance with the projectile velocity that forms an envelope to the fluid velocities. At these axial stations, the fluid velocities decay in an almost linear fashion with time as the projectile moves away. The fluctuations increase with axial distance.

Figure 4 shows fluid velocity traces at $x=7.27d$ for different radial positions from the wall and suggests that fluid is turbulent and certainly far from laminar. All of the radial positions reveal similar decay in an almost linear fashion with time. The fluid velocities at 13 ms are almost the same as the corresponding projectile velocity of 30 m/s, as expected. As the wall is approached, the relative magnitude of the fluctuations increases and fewer velocity values are recorded. This suggests that the density of scattering particles is lower than in the core of the flow. It can also be seen that the mean level of the instantaneous velocities drops close to the wall.

In order to build a picture of the flow inside the barrel at a certain time, ensemble mean and rms values need to be considered during a finite time interval and over many single realizations. The experimental sample size was chosen to be greater than 80 within a time interval of 3 ms as a compromise between the need to reduce the time gradient broadening and the number of samples necessary to obtain an acceptable statistical error. According to Ref. 10, the number of at least 80 samples ensured a maximum statistical error in the mean velocity of 2%. In the core of the flow where the sample sizes were generally greater than 120, the error is less than 1%. The corresponding error in the rms velocity is on the order of 10%.

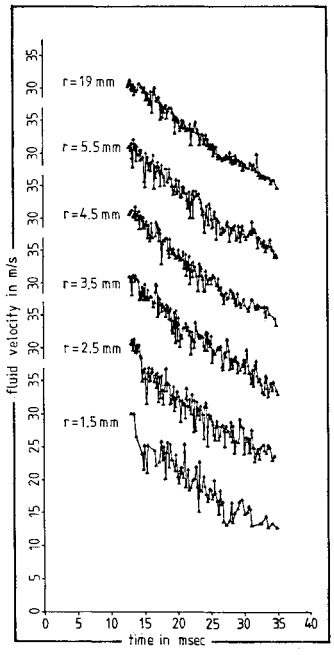

Fig. 4 Fluid velocity traces at $x=7.27d$ for different radial positions from the wall.

Other sources of error are gradient broadenings due to the variation of the velocity within the average time interval of 3 ms and within the measuring probe volume. The maximum possible error (including the accuracy of the measurement system, gradient broadenings, and statistical uncertainty) is about 4% in the mean velocity and less than 20% in the rms velocity.

Figure 5 presents radial profiles of the mean and rms axial velocity inside the barrel for a time of 26 ms at $x=7.27d$, $10.20d$, and $13.13d$ and represents the state of fluid motion when the projectile has almost reached the muzzle. The mean velocity profiles show similar trends, with a flat core that occupies almost 80% of the barrel radius. Near the wall, both the mean and rms profiles reveal the existence of a shear layer. The rms values are low over the bulk of the flow, around 4% of the local mean velocity, and increase to reach 10% of the mean velocity near the wall. Also shown in Fig. 5 is the axial distribution of the boundary-layer thickness, which increases from $0.18R$ at $x=7.27d$ to $0.21R$ at $x=10.20d$, decreases to $0.15R$ at $x=13.13d$, and should go to zero at the projectile base.

Little is known about the behavior of transient boundary layers and a comparison with steady boundary layers may be helpful. Figure 6a shows the variation of the measured boundary-layer thickness with the axial distance at a fixed time of 26 ms together with the calculated variations of a steady incompressible laminar boundary layer starting at the breech and steady incompressible turbulent boundary layers with zero and favorable pressure gradient,[11] starting at the end of the initial chamber where the boundary layers are believed to be laminar.[5] For calculations of the boundary-layer thickness with a favorable pressure gradient, a linear variation of core velocity between the breech and projectile base was used at the chosen time to evaluate the corresponding pressure gradient. The measured boundary-layer thicknesses are more closely related to the turbulent boundary layers, as shown in the figure.

Figure 6b shows the measured velocity profiles inside the boundary layer for different times and axial locations, together with 1/7 power law of turbulent steady flow inside a tube. The measured velocity profiles follow closely the 1/7 power law. The exponent for the measured profiles can be found by the least-squares technique, which gives values from 1/6.6 for the lowest bulk Reynolds number based on the diameter of the tube (which occurs at the earliest parts of the projectile motion) to 1/9.9 for the highest bulk Reynolds number (which occurs when the projectile reaches the muzzle). The calculated shape factor was 1.2–1.3 and again suggests that the measured boundary layers are turbulent.[12]

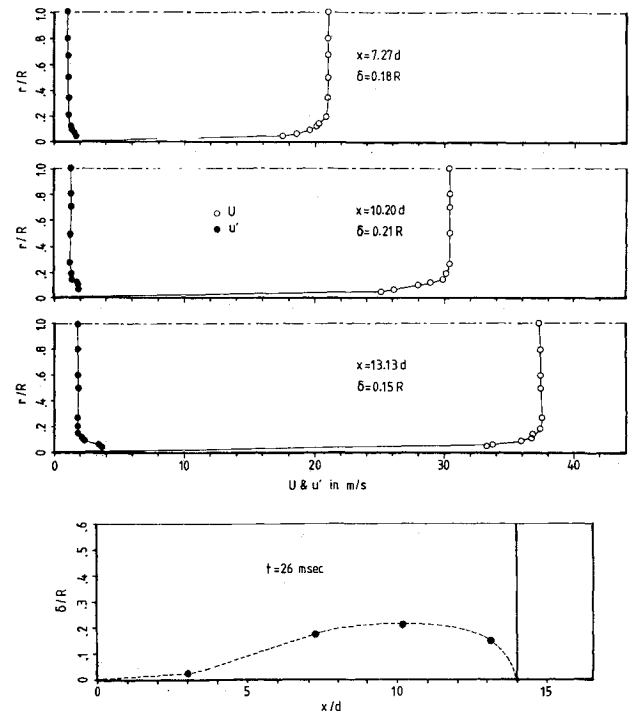

Fig. 5 Mean and rms velocity profiles at $t=26$ ms for $x=7.27d$, $10.20d$, and $13.13d$.

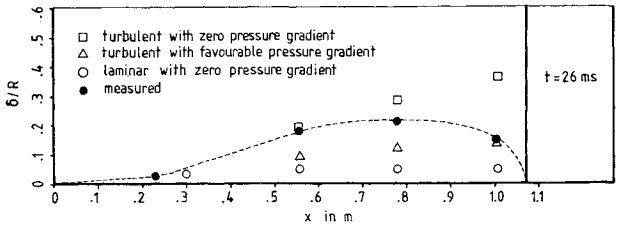

Fig. 6a Measured and calculated steady boundary-layer thicknesses.

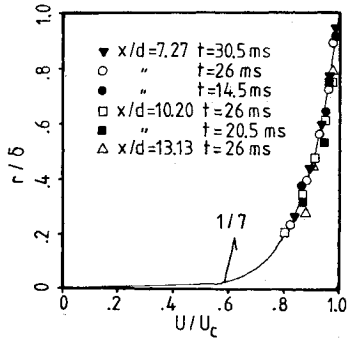

Fig. 6b Velocity distribution inside the boundary layer (line represents the 1/7 power law).

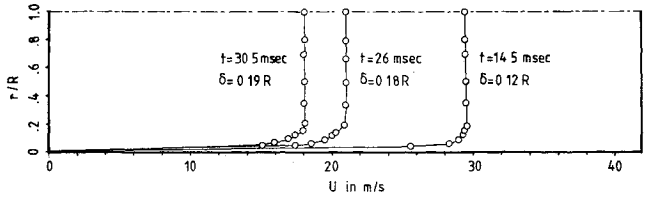

Fig. 7 Mean velocity profiles at $x=7.27d$ for different times.

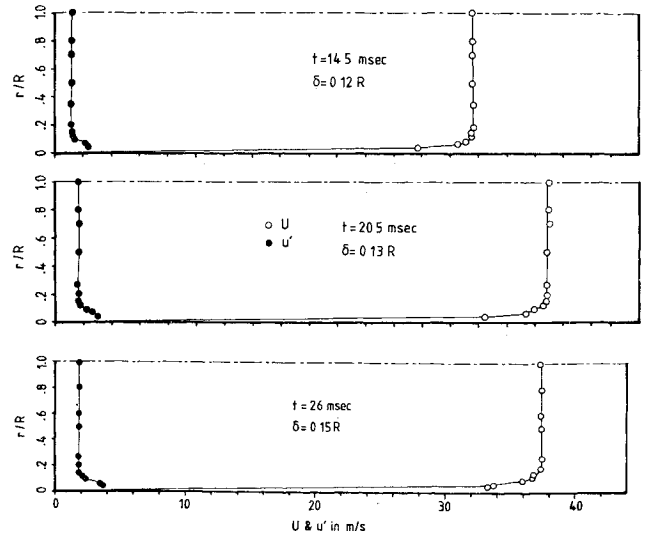

Fig. 8 Mean and rms velocity profiles at $x=z+z_0-60$ mm for different times.

Figure 7 shows the profiles of the mean axial velocity at $x=7.27d$ for three different times during the cycle of 14.5, 26, and 30.5 ms and represents the evolution of the mean axial flow with time at a fixed position (Eulerian frame). It can be seen that the boundary-layer thickness increases from $0.12R$ at 14.5 ms to $0.19R$ later in the cycle. The boundary layer at a fixed position, therefore, grows with time during the cycle and reaches an almost constant thickness. Figure 8 shows the evolution of the mean and rms axial velocity profiles at a fixed location of 60 mm behind the moving projectile, so that it represents the flow following the motion of the projectile (Lagrangian frame). In common with Fig. 7, the profiles at 14.5 ms show a boundary-layer thickness of $0.12R$, which grows, however, at a much slower rate to reach $0.13R$ at 20.5 ms and $0.15R$ at 26 ms.

Conclusions

The following main conclusions may be extracted from this investigation:

1) The relationship between the breech pressure and the projectile velocity may be determined by consideration of one-dimensional, unsteady forms of the continuity and momentum equations. The measured breech pressure record leads to calculated projectile velocity values within 0.5% of the measured ones and confirms that the friction between the projectile and the tube wall is negligible.

2) The fluid velocity traces, together with the corresponding ensemble mean and rms velocity profiles, indicate the presence of a shear layer behind the projectile that occupies around 20% of the tube radius. In the initial chamber, the boundary-layer thickness is of the order of 1% of the radius.

3) The nature of the fluid velocity fluctuations and the shape of the ensemble mean and rms velocity profiles inside the boundary layer suggest that the boundary layer is turbulent. The evolution of the boundary-layer thickness as compared to steady turbulent and laminar boundary layers shows that it is closer to the former.

Acknowledgment

Financial support provided by the U.S. Army and the Atomic Energy Research Establishment at Harwell is gratefully acknowledged. The technical assistance of Messrs. J. Laker and P. Trowell is also appreciated.

References

[1]Farrar, C. L. and Leeming, D. W., *Military Ballistics, A Basic Manual*, Brassey's Defence Publishers, London, 1983.

[2]Klingenberg, G. and Banks, N. E., "Review on Interior and Transitional Ballistic Research: State of the Art of Computational and Experimental Efforts," Ernst-Mach Institut Rept. Expl. 028, 1981.

[3]Schmitt, J. A., Banks, N. E., Zoltani, C. K., and Mann, T. L., "Two-Phase Viscous Flow Modeling of Interior Ballistics, Algorithm and Numerical Predictions of an Idealized Lagrange Gun," ASME Paper 81, Nov. 1981.

[4]Heiser, R., "Two-Phase Flow, Interior Ballistic Modeling," Paper presented at U.S. Army Workshop of Two-Phase Flows, Mechanical Engineering Dept., Fluids Section, Imperial College, London, Nov. 1985.

[5]Bicen, A. F., Kliafas, Y., and Whitelaw, J. H., "In-Bore Velocity Measurements in the Wake of a Subsonic Projectile," *AIAA Journal*, Vol. 24, 1986, p. 1035.

[6]McCroskey, W. J., "Some Current Research on Unsteady Fluid Dynamics," *Journal of Fluid Engineering*, Vol. 99, 1976.

[7]Carr, L. W., *A Review of Unsteady Turbulent Boundary Layer Experiments, in Unsteady Turbulent Shear Flows*, edited by R. Michel, J. Cousteix, and R. Houdeville, Springer-Verlag, New York, 1981, p. 3.

[8]Shapiro, A. A., *The Dynamics and Thermodynamics of Compressible Fluid Flow*, Vol. 2, Ronald Press, New York, 1953.

[9]Seigel, A. E., "Theory of High-Muzzle-Velocity Guns," *AIAA Progress in Astronautics and Aeronautics: Interior Ballistics of Guns*, Vol. 66, edited by H. Krier and M. Summerfield, AIAA, Washington, DC, 1979, p. 135.

[10]Yanta, W. J. and Smith, R. A., "Measurements of Turbulence-Transport Properties with a Laser Doppler Velocimeter," AIAA Paper 73-169, 1973.

[11]Kays, W. M. and Crawford, M. E., *Convective Heat and Mass Transfer*, McGraw-Hill, New York, 1980.

[12]Schlichting, H., *Boundary Layer Theory*, 7th ed., McGraw-Hill, New York, 1979.